Mössbauer effect in confined liquid molecules

J. Hietaniemi, T. Katila, J. Lindén, and I. Tittonen
Department of Technical Physics, Helsinki University of Technology, SF-02150 Espoo, Finland

E. Ikonen
Metrology Research Institute, Helsinki University of Technology, SF-02150 Espoo, Finland
(Received 3 February 1992)

Results of experimental and theoretical studies on the ^{119}Sn Mössbauer effect in $SnCl_4$ molecules confined in porous glass are presented. A physical model, based on the assumption that diffusion is hindered in the pores, is developed. It is further assumed that the molecules in each pore form a harmonic lattice with fixed boundary conditions. The thermal-vibration amplitudes of the particles are calculated by using a normal-mode expansion satisfying fixed boundary conditions. It is rigorously shown that the transformation diagonalizes the Hamiltonian of the system, allowing subsequent use of standard calculational methods to derive expressions for the recoilless fraction and the second-order Doppler shift in restricted geometry. The result allows evaluation of these quantities for molecules at different sites in the lattice. Experiments were made with two Vycor-glass carriers at several temperatures below and above the 240-K freezing point of bulk $SnCl_4$. The samples have average pore diameters of 40 and 36 Å. Mössbauer data of confined $SnCl_4$ reveal a resonance line shift corresponding to the solid-liquid transition. This change in isomer shift is attributed to volume expansion of $SnCl_4$ at its melting point. The measured temperature dependence of the recoilless fraction of the confined $SnCl_4$ molecules is explained by the theoretical model. With one adjustable parameter, the theory reproduces both the absolute level and the temperature slope of the experimental data for two spectral components corresponding to $SnCl_4$ molecules at different locations in the pore.

I. INTRODUCTION

Mössbauer spectroscopy can be applied to study the motion of resonant nuclei. The mean-square displacement affects the probability of recoilless absorption and emission, whereas the mean-square velocity shifts spectral lines via the second-order Doppler effect. Confining the substance under study in small void spaces of porous glass has been found to enhance the probability of recoilless absorption significantly. Bogomolov, Klushin, and Seregin studied the ^{119}Sn resonance in Sn atoms diluted in gallium metal, which was pressed into a porous glass carrier.[1,2] They attributed the enhancement of the recoilless fraction to stiffening of the phonon spectrum in the finely dispersed metal. Burger and Vertés reported on Mössbauer absorption in different iron- or tin-containing solutions.[3] These studies originated from the idea that liquids in porous media would behave as solids. Since then the phenomenon has been reported in subsequent experiments performed with pure $SnCl_4$ and its solutions.[4,5] A model has been proposed to explain the effect.[6] This model is based on geometrical properties of the pores and does not incorporate physical parameters such as interactions between the molecules or the influence of temperature. Our experiments to reproduce the Mössbauer effect in confined liquid molecules have been successful with the ^{119}Sn resonance only.[7,8] The data on the temperature dependence of the recoilless fraction in porous glass confirm the Mössbauer effect in the liquid regime.[8]

Dynamical and thermodynamical properties of molecular systems change drastically when they are confined in very small spaces, such as pores of Vycor glass.[9] Studies on the effect of restricted geometry include diffusion of molecules,[10,11] superfluid transitions,[12] and supercooling of liquids[13] using porous hosts. Because of possible practical applications of porous media, interest in their structural properties is increasing.[14–17]

In this paper, studies on the ^{119}Sn Mössbauer resonance in $SnCl_4$ molecules trapped in Vycor-glass porous hosts are presented. A simplified model, covering the essential features of the confined $SnCl_4$ molecules, is presented. The basic assumption is that diffusion is obstructed in the pores within the lifetime of the excited nuclear state. Further assumptions reduce the system to a cubic unit in which the molecules effectively form a lattice with particles connected by harmonic forces. Instead of the normal periodic boundary conditions, fixed boundary conditions are employed. Starting from the classical Hamiltonian and equations of motion, expressions for the mean-square displacement and velocity are derived to calculate the recoilless fraction and the second-order Doppler shift in restricted geometry. The results show how these quantities depend on the temperature and the

pore size. The properties of the confined molecules are described by one parameter, the Debye temperature of the lattice. Experimental data on the recoilless fraction and resonance line positions are recorded as a function of temperature using two glass carriers with different average pore sizes. The recoilless fraction in both samples is reproduced by the theory: with one adjustable parameter, the theory gives the absolute value and the temperature slope of two spectral components, attributed to confined molecules occupying unequal sites in the pores. By employing the possibility to observe the Mössbauer effect in confined $SnCl_4$ molecules above the bulk melting point, additional data on resonance line shifts corresponding to the solid-liquid transition are presented.

II. THEORY

A. Model for the pores

We consider a system consisting of an interconnected network of void spaces in porous glass filled with $SnCl_4$ molecules. A simple model to describe molecular dynamics in the pores is given to facilitate calculation of the mean-square displacement and velocity of the molecules. From these quantities, the Mössbauer recoilless fraction and the second-order Doppler shift are evaluated.

The occurrence of the Mössbauer effect shows that diffusion of the molecules is hindered in the pores. Accordingly, we make the basic assumption that any diffusive motion during the lifetime of the excited nuclear state is negligible. In addition, the complex topology of the pores is reduced to a cubic cavity where the molecules effectively form a lattice. The $SnCl_4$ molecules and the surrounding glass molecules are treated as mass points, omitting intramolecular vibrations. The thermal vibrations in the cavity are normalized to zero amplitude at the glass walls. The physical idea that lies behind the latter assumption is that the glass molecules are much less free to move than the $SnCl_4$ molecules coupled by weak liquidlike interactions.

Mathematically, the framework may be presented as a lattice consisting of $N=L^3$ particles at positions $\mathbf{l}=\sum_{\alpha=1}^{3} l_\alpha \mathbf{a}_\alpha$, where $\mathbf{a}_\alpha$'s are the primitive vectors of the lattice and $l_\alpha=0,1,\ldots,L-1$. The lattice constant is $a=|\mathbf{a}_\alpha|$. The stationary glass molecules occupy positions $l_\alpha=0$ or $L-1$ and the $SnCl_4$ molecules in contact with the walls are adjacent to the glass molecules, $l_\alpha=1$ or $L-2$. The rest of the lattice is occupied by $SnCl_4$ molecules with a nearest-neighbor environment resembling that of bulk liquid. In calculations, the interactions between the molecules up to the third-nearest-neighbor shell are taken into account using the harmonic approximation. The force between a stationary glass molecule and an adjacent $SnCl_4$ molecule is assumed to be equal to the force between two adjacent $SnCl_4$ molecules.

B. Diagonalization of the Hamiltonian

In the following, a rigorous quantum-mechanical treatment of the simplified system described in Sec. II A is given. The calculation with fixed boundary conditions is presented in detail since it is not found in standard textbooks where periodic boundary conditions are normally used. The Hamiltonian of the system is

$$H=\tfrac{1}{2}\sum_{l,\alpha} M\dot{u}_\alpha(l)^2+\tfrac{1}{2}\sum_{l,\alpha}\sum_{l',\beta}\phi_{\alpha\beta}(l,l')u_\alpha(l)u_\beta(l')\ , \tag{1}$$

where M is the mass of $SnCl_4$ *molecules*. The vectors $\mathbf{u}(l)$ with components $u_\alpha(l)$, $\alpha=1,2,3$, are the displacements of the molecules from their equilibrium positions. The dot indicates a time derivative. The quantity $\phi_{\alpha\beta}(l,l')$ represents the force acting on a particle at the position l in the α direction when a particle at l' moves a unit length in the β direction. The tensor ϕ is symmetric, i.e., $\phi_{\alpha\beta}(l,l')=\phi_{\beta\alpha}(l',l)$. As the interactions beyond the third-nearest-neighbor shell are omitted and each $SnCl_4$ molecule is acted upon by similar forces, the relation $\phi_{\alpha\beta}(l,l')=\phi_{\alpha\beta}(l-l')$ also holds. The element $\phi_{\alpha\beta}(l-l')$ is nonzero only when $l_\alpha-l'_\alpha=0$ or ±1 for each component α.

Solutions of the classical equations of motion give the eigenfrequencies $\omega_j(\mathbf{q})$ and eigenvectors $\mathbf{e}(\mathbf{q},j)$ of the system, see Appendix A. The wave vector associated with a normal mode is $\mathbf{q}$ and the index j labels the three branches. To fulfill the boundary conditions of the model, the allowed components of the wave vector are

$$q_\mu=\frac{\pi}{(L-1)a}n_\mu,\quad n_\mu=1,2,\ldots,L-2\ . \tag{2}$$

We write the displacement amplitude at the position l as a linear combination of the normal modes with amplitudes $Q(\mathbf{q},j)$,

$$u_\alpha(l)=\left[\frac{2}{L-1}\right]^{3/2}\frac{1}{\sqrt{M}}\sum_{\mathbf{q},j}e_\alpha(\mathbf{q},j)Q(\mathbf{q},j)\sin(q_1l_1a)\times\sin(q_2l_2a)\sin(q_3l_3a)\ , \tag{3}$$

where the harmonic time dependence of the vibrations is not written explicitly.

Substituting expansion (3) in Eq. (1) and using Eqs. (A3), (A5), and (A9), the Hamiltonian is diagonalized,

$$H=\tfrac{1}{2}\sum_{\mathbf{q},j}[\dot{Q}^2(\mathbf{q},j)+\omega_j^2(\mathbf{q})Q^2(\mathbf{q},j)]\ . \tag{4}$$

This Hamiltonian is of the standard form,[18] and may be quantized by introducing the phonon annihilation and creation operators

$$b_j(\mathbf{q})=\left[\frac{\omega_j(\mathbf{q})}{2\hbar}\right]^{1/2}Q(\mathbf{q},j)+i\left[\frac{1}{2\hbar\omega_j(\mathbf{q})}\right]^{1/2}\dot{Q}(\mathbf{q},j)\ , \tag{5a}$$

$$b_j^\dagger(\mathbf{q})=\left[\frac{\omega_j(\mathbf{q})}{2\hbar}\right]^{1/2}Q(\mathbf{q},j)-i\left[\frac{1}{2\hbar\omega_j(\mathbf{q})}\right]^{1/2}\dot{Q}(\mathbf{q},j)\ , \tag{5b}$$

respectively. With use of Eqs. (A5) and (A9) it is straightforward to derive the inverse transform of Eq. (3) and show that $b_j(\mathbf{q})$ and $b_j^\dagger(\mathbf{q})$ obey the boson commutation relations.

C. Recoilless fraction and second-order Doppler shift

The probability of the Mössbauer effect depends on the vibration amplitude of the emitting or absorbing nucleus via a quantity $\exp[i\mathbf{k}\cdot\mathbf{u}(l)]$, where $\mathbf{k}$ is the wave vector of the γ quantum. More precisely, the recoilless fraction is given by the square of the statistical average of the quantum-mechanical expectation value of this operator in the manifold of the vibrational states in the lattice: $f(l)=|\langle\exp[i\mathbf{k}\cdot\mathbf{u}(l)]\rangle_T|^2$.[19] In the following, a rigorous quantum-mechanical evaluation of this thermal average for the system described above is given.

According to Eqs. (3) and (5), the displacement $u_\alpha(l)$ is a linear combination of the phonon operators

$$u_\alpha(l)=\left[\frac{2}{L-1}\right]^{3/2}\sum_{\mathbf{q},j}\left[\frac{\hbar}{2M\omega_j(\mathbf{q})}\right]^{1/2}e_\alpha(\mathbf{q},j)[b_j(\mathbf{q})+b_j^\dagger(\mathbf{q})]\prod_{\mu=1}^{3}\sin(q_\mu l_\mu a)\ . \tag{6}$$

It is easy to show that the Bloch's identity[18] is valid with fixed boundary conditions, and hence

$$\langle e^{i\mathbf{k}\cdot\mathbf{u}(l)}\rangle_T=\exp[-\tfrac{1}{2}k^2\langle u_\alpha^2(l)\rangle_T]\ . \tag{7}$$

The recoilless fraction for a nucleus at the position l depends on the mean-square displacement $\langle u_\alpha^2(l)\rangle_T$ in the direction of the γ ray.

A straightforward calculation (see Appendix B) gives a result

$$\langle u_\alpha^2(l)\rangle_T=\left[\frac{2}{L-1}\right]^3\frac{\hbar}{6M}\times\sum_{\mathbf{q},j}\frac{\coth(\hbar\omega_j(\mathbf{q})/2k_BT)}{\omega_j(\mathbf{q})}\prod_{\mu=1}^{3}\sin^2(q_\mu l_\mu a)\ . \tag{8}$$

As compared with the corresponding expression with periodic boundary conditions,[18] this equation includes the squared basis functions of the normal-mode expansion (3) explicitly. The sum over the wave vector $\mathbf{q}$ is limited to values indicated in Eq. (2), instead of the first Brillouin zone. For a molecule located at the center of the pore, the present result approaches that obtained with periodic boundary conditions when $L\to\infty$. It is seen that the recoilless fraction in restricted geometry is always larger than that of the corresponding bulk material.

The observed recoilless fraction is an average of the contributions from the appropriate positions l. For the particles located in the central part of the cavity, the recoilless fraction is

$$f_m=\frac{1}{(L-4)^3}\sum_{l_1=2}^{L-3}\sum_{l_2=2}^{L-3}\sum_{l_3=2}^{L-3}\exp[-k^2\langle u_\alpha^2(l)\rangle_T]\ . \tag{9}$$

For the molecules at the walls, l_α values corresponding to the glass-$SnCl_4$ interface, excluding edge and corner positions, are included in the average. To evaluate numerically the sums indicated in Eq. (8), the Debye approximation scheme is adopted. For each branch, a linear dispersion relation $\omega_j(\mathbf{q})=c_v|\mathbf{q}|$ is used where c_v is the velocity of sound in the lattice. The lattice is characterized by a Debye temperature related to c_v by $\Theta=(6\pi^2)^{1/3}\hbar c_v/(k_Ba)$.[20]

The thermal vibration of nuclei affects the energy of the γ rays via the second-order Doppler effect. The velocity $\dot{\mathbf{u}}(l)$ of a nucleus gives rise to a relative energy change of $-\langle\dot{\mathbf{u}}^2(l)\rangle_T/(2c^2)$, where c is the velocity of light. The mean-square velocity due to the molecular motion in the restricted geometry may be evaluated in the same way as $\langle u_\alpha^2(l)\rangle_T$. The normal-mode expansion of $u_\alpha(l)$ is replaced by the corresponding expression for the velocity,

$$\dot{u}_\alpha(l)=-i\left[\frac{2}{L-1}\right]^{3/2}\sum_{\mathbf{q},j}\left[\frac{\hbar\omega_j(\mathbf{q})}{2M}\right]^{1/2}e_\alpha(\mathbf{q},j)[b_j(\mathbf{q})-b_j^\dagger(\mathbf{q})]\prod_{\mu=1}^{3}\sin(q_\mu l_\mu a)\ . \tag{10}$$

For an isotropic lattice, the resulting second-order Doppler shift in velocity units is

$$-3\langle\dot{u}_\alpha^2(l)\rangle_T/2c=-\left[\frac{2}{L-1}\right]^3\frac{1}{4Mc}\sum_{\mathbf{q},j}\hbar\omega_j(\mathbf{q})\coth\left[\frac{\hbar\omega_j(\mathbf{q})}{2k_BT}\right]\prod_{\mu=1}^{3}\sin^2(q_\mu l_\mu a)\ . \tag{11}$$

For a particle at the center of the pore, Eq. (11) produces in the limit $L\to\infty$ the same value as the expression obtained with periodic boundary conditions. In finite-size pores, the magnitude of the line shift of Eq. (11) is always smaller than that for the corresponding bulk material.

The weight factor in the equation for the mean-square displacement [Eq. (8)] is $1/\omega_j(\mathbf{q})$, whereas in Eq. (11) it is $\omega_j(\mathbf{q})$. Thus, the recoilless fraction and the second-order

Doppler shift achieve their major contributions from the low-frequency and the high-frequency parts of the phonon spectrum, respectively. It is expected that the restricted geometry in the pores does not affect the short-wavelength part of the phonon spectrum. Thus, the influence of confinement is mainly reflected in the recoilless fraction, but not much in the second-order Doppler shift.

III. EXPERIMENT

In the experiments, the 23.9-keV Mössbauer resonance of ^{119}Sn was used. The experiments with the porous glass carriers were performed using a ^{119}Sn:$CaSnO_3$ source, whereas in the auxiliary measurements with frozen bulk $SnCl_4$, the source was ^{119}Sn:$BaSnO_3$. The isomer shifts of these source matrices are equal to that of SnO_2. The recoilless fraction is 0.57 for the $CaSnO_3$ matrix and 0.62 for the $BaSnO_3$ matrix.[21] To increase the signal-to-noise ratio at the NaI detector, the x rays of Sn were filtered using thin palladium foils.

The absorbers were made of 1.5-mm-thick plates of porous glass.[22] According to the manufacturer, the glass has a porosity of 28%. The void spaces in the glass are longish cavities with a complex geometry.[10] If a cylindrical shape is assumed for the pores, their average cross section is 40 Å in diameter. To study the influence of the pore size on the Mössbauer effect, some of the glass carriers were heated at 1000 °C to reduce the void spaces. At this temperature, an irreducible linear shrinkage of 10% of the pores is specified. In the following the nonheated glass will be referred to as sample *A* and the heat-treated glass as sample *B*.

The pieces of glass were cleaned using the standard procedure described by the manufacturer. Then the glass carriers were allowed to soak in pure liquid $SnCl_4$ for 20 h to make sure that the pores were filled with $SnCl_4$. It was checked by weighing that the samples absorbed an amount of $SnCl_4$ corresponding to their porosity. Finally, the absorbers were enclosed in air-tight sample holders as shown in Fig. 1. To ensure that the sample remains impregnated with $SnCl_4$, the piece of glass was surrounded by excess $SnCl_4$. The total thicknesses of the bulk layers were 1.0 and 1.5 mm with samples *A* and *B*, respectively. Below the freezing point $T_0 = 240$ K, frozen $SnCl_4$ gives rise to a background effect which must be taken into account in the data analysis. Auxiliary measurements of bulk $SnCl_4$ were carried out without the porous glass. In these measurements the thickness of the $SnCl_4$ layer was 3.0 mm.

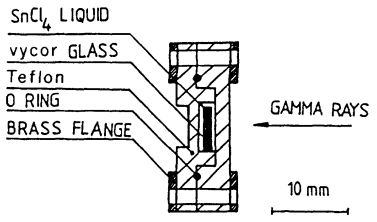

FIG. 1. Sample holder used in the experiments.

IV. RESULTS AND DISCUSSION

A. Experimental results

Spectra of frozen bulk $SnCl_4$ were measured at several temperatures between 180 and 239 K. Figure 2 shows data obtained at 239 and 180 K. The slightly asymmetric line shape was taken into account by an asymmetric pattern consisting of two Lorentzian lines. The fixed distance between the lines was 0.75 mm/s and their intensity ratio was 0.1. The fitting results are collected in Table I.

Mössbauer spectra of $SnCl_4$ trapped in pores of Vycor glass, measured at several temperatures above and below the freezing point $T_0 = 240$ K of $SnCl_4$, are shown in Fig. 3 for sample *A* and in Fig. 4 for sample *B*. The spectra were fitted using two independent Lorentzian lines. In fitting the data for temperatures below T_0, the bulk background was accounted for by using a third component with all parameters fixed to values obtained from the auxiliary bulk measurements and the thicknesses of the bulk $SnCl_4$ layers. The Mössbauer parameters obtained from the least-squares fits are summarized in Tables II and III for samples *A* and *B*, respectively.

The spectra measured using porous glass have two major components, one resonance line at about zero Doppler velocity and the other line at 0.8–0.9 mm/s. In the following we refer to them as components 1 and 2, respectively. Figure 5 shows the spectral areas of these components as a function of temperature for the samples *A* and *B*. For comparison, also the spectral area of the bulk contribution in the measurements with sample *A* is shown. The line positions obtained from samples *A* and *B* and from frozen bulk $SnCl_4$ are shown in Fig. 6.

The results presented in Figs. 3–5 show that the Mössbauer effect is observed in liquid molecules in the restricted geometry. Below T_0, Mössbauer absorption is due to all ^{119}Sn nuclei in the sample holder. Using the auxiliary bulk data, we know which portion of the effect arises from the frozen $SnCl_4$ outside the porous glass. The rest of the Mössbauer absorption must be attributed to $SnCl_4$ in the glass carrier. Above T_0, only these mole-

TABLE I. Mössbauer parameters obtained from the bulk $SnCl_4$ sample at different temperatures. The quantities *E* and *A* denote the position of the major spectral component and the total area, respectively. The spectral area is represented by the product of the linewidth and the absorption depth. Statistical errors are given in parentheses. An asterisk denotes a fixed parameter in the fitting.

T (K)	*E* (mm/s)	*A* (% mm/s)
180	0.78(1)	3.86(17)
190	0.77(1)	2.97(13)
210	0.74(1)	2.05(11)
223	0.74(2)	1.35(10)
235	0.72(2)	0.93(7)
239	0.71*	0.69(11)

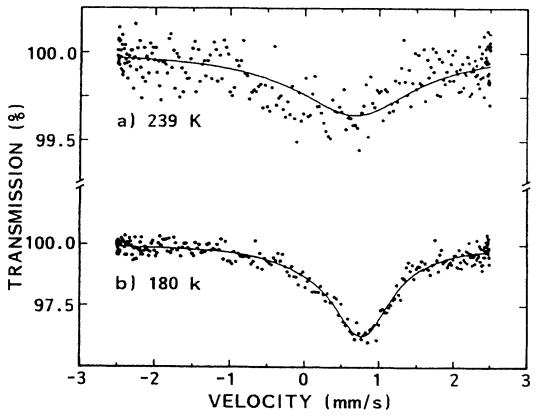

FIG. 2. Mössbauer spectra of frozen bulk $SnCl_4$ at (a) 239 K and (b) 180 K. The source was $^{119}Sn:BaSnO_3$ at room temperature. The solid lines are least-squares fits.

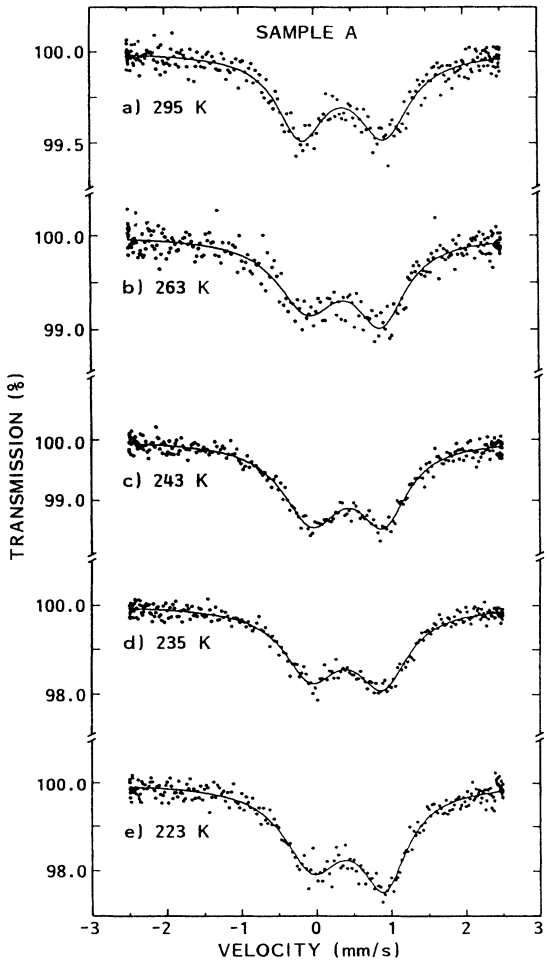

FIG. 3. Mössbauer spectra of $SnCl_4$ trapped into pores of sample *A*. The absorber temperatures were (a) 295 K, (b) 263 K, (c) 243 K, (d) 235 K, and (e) 223 K. The source was $^{119}Sn:CaSnO_3$ at room temperature.

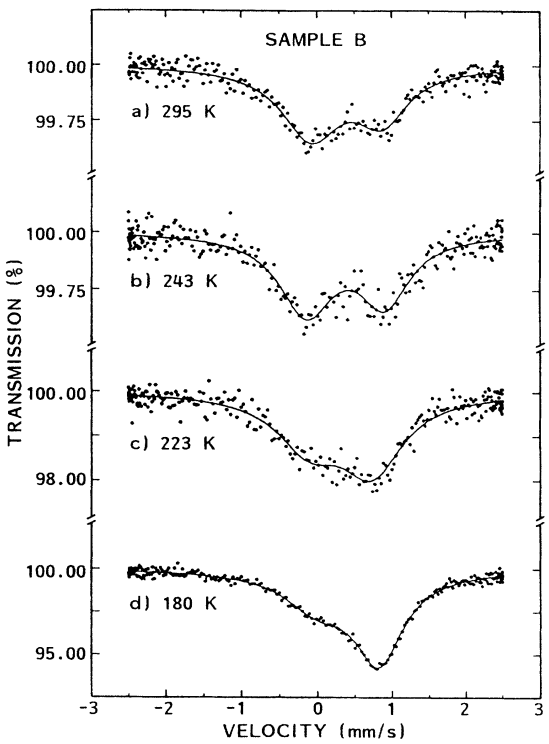

FIG. 4. Mössbauer spectra of $SnCl_4$ trapped into pores of sample *B*. The absorber temperatures were (a) 295 K, (b) 243 K, (c) 223 K, (d) 180 K. The source was $^{119}Sn:CaSnO_3$ at room temperature.

cules contribute to the Mössbauer absorption. From the weighing results it is known that the pores are filled with $SnCl_4$ molecules. It can be estimated that about one-half of them occupy the central space of the pores and are not in direct contact with the walls. The nearest-neighbor environment of these molecules resembles that of bulk

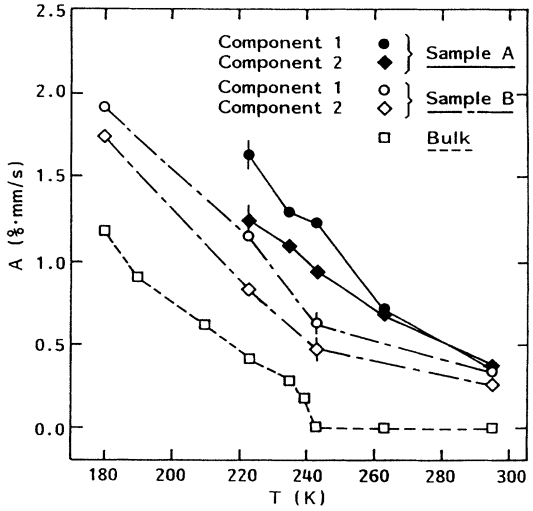

FIG. 5. Spectral areas as a function of temperature. The bulk contribution is shown for measurements with sample *A*. As a guide to the eye, the data points are connected.

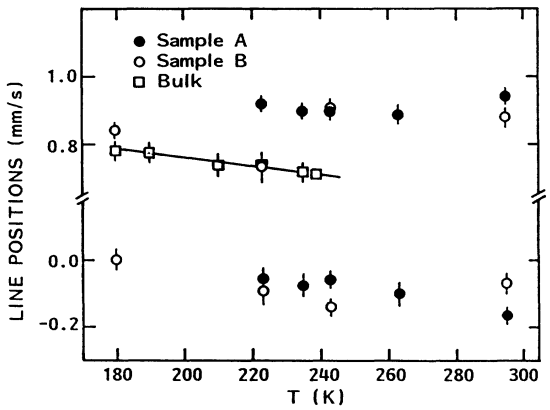

FIG. 6. Resonance line positions relative to SnO_2 as a function of temperature. The line at higher velocities shows an indication of the solid-liquid transition in porous glass.

liquid. The recoilless absorption of the central-pore component surviving above T_0 allows extension of Mössbauer studies into the liquid regime.

B. Comparison of theory and data

To allow comparison of the experimental and the theoretical results, we make a straightforward assignment for the two spectral components of confined $SnCl_4$.[5] The environment of the $SnCl_4$ molecules at the glass walls is dynamically and chemically different from that of the molecules which are located in the center space of the pore. The nearest-neighbor environment of the molecules occupying the central space of the pore should resemble that of bulk liquid molecules. The line positions of the bulk data and component 2 of the porous-glass data are close to each other, and thus we assign this line to the molecules in the central part of the pore. Component 1 is then attributed to the $SnCl_4$ molecules at the walls of the pores. The spectra of samples A and B above 240 K support the site assignment: The relative amount of the molecules at the glass walls in sample B is expected to be larger than in sample A. This is corroborated by the increased absorption of the spectral component 1 in Fig. 4 as compared with Fig. 3.

The resonance line of frozen bulk $SnCl_4$ shifts towards negative velocities when the temperature increases (see Fig. 6). The slope of -1.2×10^{-3} mm/s K is indicated by the solid line. The temperature slope of component 1 for both porous glass samples resembles that of bulk $SnCl_4$. For component 2, two levels of isomer shift values exist at about 0.8 and 0.9 mm/s. An obvious conclusion is to associate these two values with solid and liquid $SnCl_4$. The higher values of isomer shift have been measured with descending temperatures, whereas the lower values correspond to increasing temperatures. The apparent hysteresis in the isomer shift is compatible with the observed hysteresis between freezing and melting in porous glass.[13]

It may be assumed that the relative change in the valence electron density $\Delta\rho(0)$ at Sn nuclei is equal to the 12% density change of $SnCl_4$ at its melting point. With use of values from Ref. 23 for $\Delta\rho(0)$ and for the fractional variation in the nuclear radius, an order-of-magnitude estimate of 0.2 mm/s is obtained for the isomer shift difference between solid and liquid phases. This estimate is in agreement with the experimental value.

The recoilless fraction f of a thin absorber is related to the spectral area by

$$A=\tfrac{1}{2}tna\sigma_0 W_0 F_s f \ . \tag{12}$$

Parameter t is the thickness of the absorbing material layer, n the density of Sn atoms in $SnCl_4$, $\sigma_0=1.40\times10^{-18}$ cm^2 the resonant absorption cross section for ^{119}Sn, $a=0.0858$ the isotopic abundance of ^{119}Sn, and $W_0=0.647$ mm/s the natural linewidth [full width at half maximum (FWHM)]. The background-corrected recoilless fractions of the sources are $F_s=0.46$ and 0.50 for the $CaSnO_3$ and the $BaSnO_3$ matrices, respectively. For data obtained with the porous-glass samples, Eq. (12) is evaluated by taking into account the porosity of the sample and the relative amounts of $SnCl_4$ molecules with different nearest-neighbor environments; see Table IV. The latter value is obtained by a simple geometrical argument using known values of the pore radius and the molecular radius.

TABLE II. Mössbauer parameters obtained from sample A at different temperatures. Parameters E_k and A_k denote the line positions and the areas of the components $k=1$ or 2.

T (K)	E_1 (mm/s)	A_1 (% mm/s)	E_2 (mm/s)	A_2 (% mm/s)
223	−0.06(2)	1.63(12)	0.92(1)	1.25(9)
235	−0.08(2)	1.29(8)	0.90(1)	1.10(7)
243	−0.06(2)	1.23(7)	0.90(1)	0.95(6)
263	−0.10(3)	0.72(8)	0.89(2)	0.68(7)
295	−0.16(2)	0.34(3)	0.94(2)	0.37(3)

TABLE III. Mössbauer parameters obtained from sample B at different temperatures. The notation is the same as in Table II.

T (K)	E_1 (mm/s)	A_1 (% mm/s)	E_2 (mm/s)	A_2 (% mm/s)
180	0.00(3)	1.92(16)	0.84(1)	1.75(11)
223	−0.09(4)	1.15(16)	0.74(4)	0.84(10)
243	−0.14(2)	0.60(6)	0.91(2)	0.48(5)
295	−0.07(2)	0.30(2)	0.88(3)	0.27(3)

TABLE IV. Glass carrier porosities and relative amounts of the molecules in the two different environments in the pores. Values for the sample B are obtained from the linear shrinkage of 10%.

Sample	Porosity (%)	Fraction of component 1	Fraction of component 2
A	28	0.42	0.58
B	20	0.48	0.52

Within the harmonic approximation for the atomic and the molecular motions, the experimental recoilless fraction f may be decomposed as $f = f_{Sn} f_m f_{sur}$. The factor f_{Sn} accounts for vibration of the Sn atom within the $SnCl_4$ molecule, f_m is related to motion of the $SnCl_4$ molecules, and f_{sur} comprises the effect of the surrounding glass walls. The theory of Sec. II deals with the factor f_m. We estimate the small contributions of f_{Sn} and f_{sur} as follows: The temperature-independent factor $f_{Sn} = 0.735$ may be obtained from the data on intramolecular mean-square displacements.[24] The temperature-dependent contribution f_{sur} may be calculated by adding the mean-square displacements of the glass molecules to those of the $SnCl_4$ molecules at the walls using a coupling proportional to their mass ratio. The motion of molecules in the central part of the pore is assumed to be insensitive to the glass vibrations because of low acoustic coupling between glass and $SnCl_4$. The mean-square displacements of the glass molecules were evaluated using a Debye temperature of 370 K, obtained from the velocity of sound in SiO_2.[25] Between 180 K and room temperature this correction varies from 0.89 to 0.83. Values of the recoilless fraction f_m for the confined and bulk $SnCl_4$ are presented in Table V.

There is a significant enhancement in the recoilless fraction in confined $SnCl_4$ as compared with that of frozen bulk material. In Table V, the apparent enhancement factor is more than 10. The theory of Sec. II predicts a factor of only ~ 3 around 240 K. However, the theoretical description does not take into account collective molecular motion in bulk $SnCl_4$ which increases strongly near the melting point. The confinement prevents motion of large molecular clusters leading to Mössbauer absorption even above 240 K.

The data points in Figs. 7 and 8 show the temperature dependence of $-\ln f_m$ for the components 1 and 2 of samples A and B. The solid lines indicate the corresponding quantity evaluated using the theory of Sec. II. For sample A, a lattice size of $N = 10^3$ and a Debye temperature of $\Theta = 58$ K are used. The corresponding values for sample B are $N = 9^3$ and $\Theta = 57$ K. For both samples, agreement between the data and the theoretical prediction is good: with one adjusted parameter (Θ) whose values for the two samples closely agree, the model reproduces the absolute values of the data points and the temperature slopes for both spectral components.

The error bars in Figs. 7 and 8 include statistical uncertainties only. The main source of systematic error is

TABLE V. Recoilless fractions f_m in percent for confined and bulk $SnCl_4$ at different temperatures. The components are denoted as in Tables II and III. The uncertainties include the statistical errors only.

	Sample A		Sample B		Bulk
T (K)	1	2	1	2	$SnCl_4$
180	...	...	2.18(18)	1.61(10)	0.145(6)
190	...	...	...	...	0.111(5)
210	...	...	...	...	0.077(4)
223	1.50(12)	0.72(5)	1.35(18)	0.77(9)	0.051(3)
235	1.20(8)	0.64(4)	...	...	0.035(3)
239	...	...	...	...	0.026(4)
243	1.15(7)	0.55(4)	0.71(7)	0.44(4)	...
263	0.69(8)	0.39(4)	...	...	...
295	0.33(3)	0.22(2)	0.37(3)	0.25(3)	...

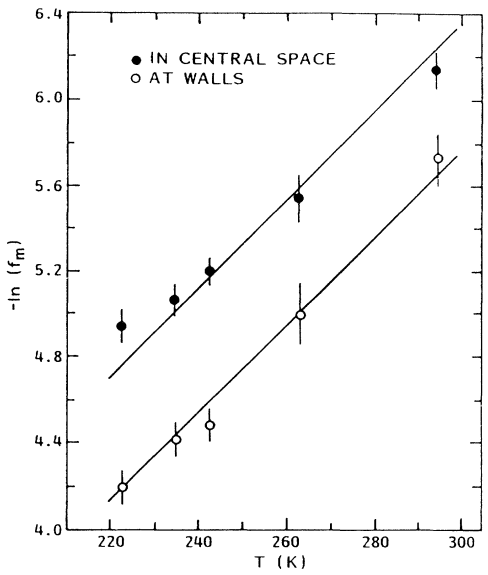

FIG. 7. Temperature dependence of the recoilless fraction f_m related to confined molecules in sample A. The negative logarithm of f_m is plotted. Error bars indicate the statistical uncertainty of the data points. The solid lines are predictions of the theory calculated using a Debye temperature of 58 K. The pore is assumed to consist of $N = 10^3$ molecules.

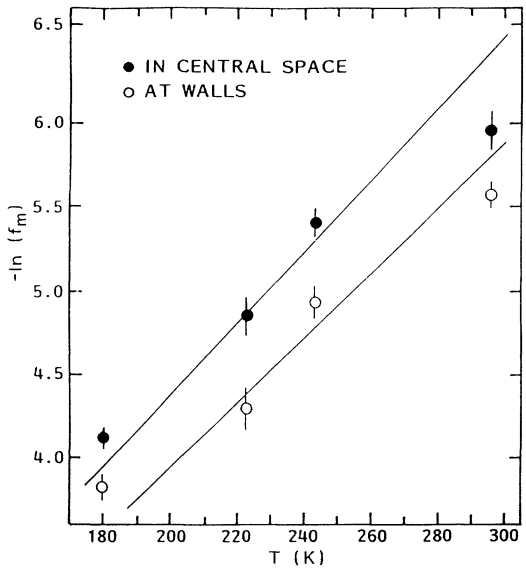

FIG. 8. Temperature dependence of the recoilless fraction f_m related to confined molecules in sample B. The negative logarithm of f_m is plotted. Error bars indicate the statistical uncertainty of the data points. The solid lines are predictions of the theory calculated using a Debye temperature of 57 K. The pore is assumed to consist of $N = 9^3$ molecules.

the estimated relative uncertainty of ~20% in the fractions of the molecules with the two different environments. Uncertainties in the porosity, in the corrections relating the recoilless fractions f and f_m, and in the signal-to-noise ratio of the pulse-height spectrum are about 10%. With some smaller additional contributions, the total systematic uncertainty is estimated to be about three times the statistical uncertainty. However, the systematic errors are approximately equal at different temperatures and thus they do not affect the relative positions of the data points.

V. SUMMARY

Experimental and theoretical studies on the Mössbauer effect in $SnCl_4$ molecules confined in porous glass are presented. Using physical arguments, the actually very complex system is reduced to a cubic lattice. The molecules are treated as vibrating mass points connected by harmonic forces. The amplitudes are normalized to zero at the stationary glass boundaries. The theoretical approach is based on the classical Hamiltonian and classical equations of motion which yield the normal modes of the system. The thermal displacement amplitudes of the particles are presented as a linear combination of the normal modes, satisfying fixed boundary conditions. The orthonormality properties of the present normal-mode expansion diagonalize the Hamiltonian, thus allowing subsequent use of standard calculational procedures. Expressions are derived for the recoilless fraction and the second-order Doppler shift arising from the molecular motion in restricted geometry.

Experimental data are obtained from ^{119}Sn Mössbauer measurements using two $SnCl_4$-containing glass carriers at several temperatures below and above the bulk freezing point of 240 K. The data obtained confirm existence of Mössbauer absorption in confined $SnCl_4$ liquid above 240 K. The Mössbauer effect of confined liquid is applied to study the recoilless fraction and the resonance line positions in the solid-liquid transition regime. A change in the isomer shift is explained by volume expansion of $SnCl_4$ at its melting point.

From the experimental data on the recoilless fraction of confined $SnCl_4$, the recoilless fraction f_m attributed to the molecular motion only is extracted. Corrections due to the intramolecular motion and influence of the glass matrix are taken into account in the analysis. The temperature dependence of f_m is compared with the theoretical prediction. For both samples the agreement is good: with one adjustable parameter, the theory reproduces both the absolute level and the temperature slope of the two spectral components.

ACKNOWLEDGMENTS

The authors express their gratitude to Professor L. Niinistö, Mrs. Tarja Koskentalo, and Mrs. Maarit Karppinen from the Laboratory of Inorganic and Analytical Chemistry of the Helsinki Univeristy of Technology for the preparation of the samples, and to Mr. M. Lippmaa for his skillful assistance during the experiments. We wish to thank Dr. E. Realo from the Institute of Physics of the Estonian Academy of Sciences for providing a ^{119}Sn Mössbauer source for some of the experiments. Financial support of the Academy of Finland is gratefully acknowledged. Two of us (J.H. and I.T.) thank the Wihuri Foundation for partial support.

APPENDIX A

In this appendix, the classical equations of motion are considered with fixed boundary conditions. The treatment is based on the orthogonality properties of the sinusoidal basis functions. The equations of motion for the system governed by the Hamiltonian (1) are

$$M\ddot{u}_\alpha(l)=-\sum_{l',\beta}\phi_{\alpha\beta}(l-l')u_\beta(l')\ . \tag{A1}$$

With a trial solution at the frequency ω

$$u_\alpha(l)=e_\alpha\prod_{\mu=1}^{3}\sin(q_\mu l_\mu a)\exp(-i\omega t)\ , \tag{A2}$$

one obtains

$$M\omega^2 e_\alpha\prod_{\mu=1}^{3}\sin(q_\mu l_\mu a)=\sum_{l',\beta}\phi_{\alpha\beta}(l-l')e_\beta\prod_{\mu=1}^{3}\sin(q_\mu l'_\mu a)\ , \tag{A3}$$

where e_α's are initially unknown amplitudes. To fulfill the boundary conditions of the problem, the solutions are restricted to values $q_\mu=\pi n_\mu/[(L-1)a]$, with the integers n_μ running from 1 to $L-2$. Multiplying Eq. (A3) by a factor $\prod_{\mu=1}^{3}\sin(q_\mu l_\mu a)$ and summing over the vector l, we get

$$M\omega^2 e_\alpha\left[\frac{L-1}{2}\right]^3=\sum_{l}\sum_{l',\beta}\phi_{\alpha\beta}(l-l')e_\beta\times\prod_{\mu=1}^{3}\sin(q_\mu l'_\mu a)\sin(q_\mu l_\mu a)\ . \tag{A4}$$

Here the orthonormality property

$$\frac{2}{L-1}\sum_{l_\mu=1}^{L-2}\sin(q_\mu l_\mu a)\sin(q'_\mu l_\mu a)=\delta_{q_\mu q'_\mu} \tag{A5}$$

of the basis functions of Eq. (A2) is used. We define a vector $l''=l-l'$, transforming Eq. (A4) to

$$M\omega^2 e_\alpha\left[\frac{L-1}{2}\right]^3=\sum_{\beta}\sum_{l''}\phi_{\alpha\beta}(l'')e_\beta\prod_{\mu=1}^{3}\sum_{l_\mu=1}^{L-2}\sin(q_\mu l_\mu a)\times\sin[q_\mu(l_\mu-l''_\mu)a]\ . \tag{A6}$$

Employing Eq. (A5) and a relation

$$\sum_{l_\mu=1}^{L-2}\sin(q_\mu l_\mu a)\cos(q_\mu l_\mu a)=0\ , \tag{A7}$$

the following result is obtained:

$$\omega^2 e_\alpha = \sum_\beta \left[\frac{1}{M} \sum_{l''} \phi_{\alpha\beta}(l'') \prod_{\mu=1}^{3} \cos(q_\mu l''_\mu a) \right] e_\beta \equiv \sum_\beta D_{\alpha\beta}(\mathbf{q}) e_\beta , \quad \text{(A8)}$$

where the quantity in the square brackets defines the dynamical matrix $D_{\alpha\beta}(\mathbf{q})$ of the system. For each $\mathbf{q}$ in the eigenvalue problem of Eq. (A8), the matrix $D_{\alpha\beta}(\mathbf{q})$ has three real eigenvalues $\omega_j^2(\mathbf{q})$, labeled by the branch index $j=1,2,3$. The components $e_\alpha(\mathbf{q}j)$ define the corresponding eigenvectors $\mathbf{e}(\mathbf{q}j)$ which are orthogonal and normalized by

$$\sum_{\alpha=1}^{3} e_\alpha(\mathbf{q},j) e_\alpha(\mathbf{q},j') = \delta_{jj'} . \quad \text{(A9)}$$

APPENDIX B

In this Appendix, the derivation of Eq. (8) is outlined. We denote the eigenstates of the number operator $b_j^\dagger(\mathbf{q})b_j(\mathbf{q})$ by $|\{\nu_{\mathbf{q}j}\}\rangle$: $b_j^\dagger(\mathbf{q})b_j(\mathbf{q})|\{\nu_{\mathbf{q}j}\}\rangle = \nu_{\mathbf{q}j}|\{\nu_{\mathbf{q}j}\}\rangle$. The mean-square displacements are calculated as a weighted average over these states

$$\langle u_\alpha^2(l)\rangle_T = \sum_{\{\nu_{\mathbf{q}j}\}} W_{\{\nu_{\mathbf{q}j}\}} \langle \{\nu_{\mathbf{q}j}\}|u_\alpha(l)^2|\{\nu_{\mathbf{q}j}\}\rangle . \quad \text{(B1)}$$

The Boltzman factor of the state $|\{\nu_{\mathbf{q}j}\}\rangle$ is

$$W_{\{\nu_{\mathbf{q}j}\}} = \prod_{\mathbf{q},j} e^{-\beta\hbar\omega_j(\mathbf{q})\nu_{\mathbf{q}j}} (1 - e^{-\beta\hbar\omega_j(\mathbf{q})}) , \quad \text{(B2)}$$

where $\beta = 1/(k_B T)$, and the quantum-mechanical average based on Eq. (6) is

$$\langle \{\nu_{\mathbf{q}j}\}|u_\alpha(l)^2|\{\nu_{\mathbf{q}j}\}\rangle = \left[\frac{2}{L-1} \right]^3 \frac{\hbar}{2M} \sum_{\mathbf{q},j} \frac{1}{\omega_j(\mathbf{q})} e_\alpha^2(\mathbf{q},j)(2\nu_{\mathbf{q}j}+1) \prod_{\mu=1}^{3} \sin^2(q_\mu l_\mu a) . \quad \text{(B3)}$$

Performing the summing over all possible populations $\{\nu_{\mathbf{q}j}\}$, Eq. (B1) becomes

$$\langle u_\alpha^2(l)\rangle_T = \left[\frac{2}{L-1} \right]^3 \frac{\hbar}{2M} \sum_{\mathbf{q},j} e_\alpha^2(\mathbf{q},j) \frac{\coth[\frac{1}{2}\beta\hbar\omega_j(\mathbf{q})]}{\omega_j(\mathbf{q})} \prod_{\mu=1}^{3} \sin^2(q_\mu l_\mu a) . \quad \text{(B4)}$$

In a lattice with cubic symmetry summing over $e_\alpha^2(\mathbf{q},j)$ yields a factor $\frac{1}{3}$,[26] which gives the result of Eq. (8).

[1] V. N. Bogomolov, N. A. Klushin, and P. P. Seregin, Fiz. Tverd. Tela (Leningrad) **14**, 2000 (1972) [Sov. Phys. Solid State **14**, 1729 (1973)].

[2] V. N. Bogomolov and N. A. Klushin, Fiz. Tverd. Tela (Leningrad) **15**, 514 (1973) [Sov. Phys. Solid State **15**, 257 (1973)].

[3] K. Burger and A. Vertés, Nature (London) **306**, 353 (1983).

[4] K. Burger, A. Vertés, M. Suba, and I. Dekany, Inorg. Chim. Acta **100**, 17 (1985).

[5] K. Burger, Spectrochim. Acta Part A **43**, 1105 (1987).

[6] A. Vertés, K. Burger, L. Takács, and I. Horváth, J. Radioanal. Nucl. Chem. Lett. **86**, 195 (1984).

[7] J. Hietaniemi, E. Ikonen, T. Katila, T. Koskentalo, L. Niinistö, and I. Tittonen, Hyperfine Interact. **56**, 1689 (1990).

[8] J. Hietaniemi, E. Ikonen, and T. Katila, Europhys. Lett. **18**, 373 (1992).

[9] J. M. Drake and J. Klafter, Phys. Today **43** (5), 46 (1990).

[10] W. D. Dozier, J. M. Drake, and J. Klafter, Phys. Rev. Lett. **56**, 197 (1986).

[11] M. Sahimi and V. L. Jue, Phys. Rev. Lett. **62**, 629 (1989).

[12] A. Khunara, Phys. Today **42** (7), 21 (1989).

[13] J. Warnock, D. D. Awschalom, and M. W. Shafer, Phys. Rev. Lett. **57**, 1753 (1986).

[14] P. Wiltzius, F. S. Bates, S. B. Dierker, and G. D. Wignall, Phys. Rev. A **36**, 2991 (1987).

[15] A. Höhr, H.-B. Neumann, P. W. Schmidt, P. Pfeifer, and D. Avnir, Phys. Rev. B **38**, 1462 (1988).

[16] R. F. Cook, Phys. Rev. B **39**, 2811 (1989).

[17] F. D'Orazio, J. C. Tarczon, W. P. Halperin, K. Eguchi, and T. Misuzaki, J. Appl. Phys. **65**, 742 (1989).

[18] A. A. Maradudin, E. W. Montroll, and G. H. Weiss, in *Solid State Physics*, edited by F. Seitz and D. Turnbull (Academic, New York, 1963), Vol. 3.

[19] H. J. Lipkin, Ann. Phys. (N.Y.) **26**, 115 (1964).

[20] J. R. Christman, *Fundamentals of Solid State Physics* (Wiley, New York, 1988).

[21] *Handbook of Spectroscopy*, edited by J. W. Robinson (CRC, Boca Raton, 1981), Vol. III.

[22] Vycor glass no. 7930, Corning, Inc., N.Y.

[23] M. Grodzicki, V. Männing, A. X. Trautwein, and J. M. Friedt, J. Phys. B **20**, 5595 (1987).

[24] *Gmelins Handbuch der anorganischen Chemie* (Verlag Chemie GmbH, Weinheim, 1972), Vol. 4.

[25] *Handbook of Physics and Chemistry*, edited by R. W. Weast (CRC, Cleveland, 1974).

[26] B. Donovan and J. F. Angress, *Lattice Vibrations* (Chapman and Hall, London, 1971).